Annals of Physics 375 (2016) 368–377

Contents lists available at ScienceDirect

Annals of Physics

journal homepage: www.elsevier.com/locate/aop

Topological defect formation in rotating binary dipolar Bose–Einstein condensate

Xiao-Fei Zhang [a,b,c,*], Wei Han [a], Hai-Feng Jiang [a,b], Wu-Ming Liu [d], Hiroki Saito [c], Shou-Gang Zhang [a,b]

[a] *Key Laboratory of Time and Frequency Primary Standards, National Time Service Center, Chinese Academy of Sciences, Xi'an 710600, China*

[b] *University of Chinese Academy of Sciences, Beijing 100049, China*

[c] *Department of Engineering Science, University of Electro-Communications, Tokyo 182-8585, Japan*

[d] *Beijing National Laboratory for Condensed Matter Physics, Institute of Physics, Chinese Academy of Sciences, Beijing 100190, China*

HIGHLIGHTS

- Effects of both strength and orientation of the dipoles are discussed.
- Various topological defects can be formed in different parameter regions.
- Present one possible way to obtain regular arrangements of spin textures.

ARTICLE INFO

Article history:
Received 23 May 2016
Accepted 17 October 2016
Available online 25 October 2016

Keywords:
Topological defect
Spin-dependent optical lattices
Dipolar Bose–Einstein condensate

ABSTRACT

We investigate the topological defects and spin structures of a rotating binary Bose–Einstein condensate, which consists of both dipolar and scalar bosonic atoms confined in spin-dependent optical lattices, for an arbitrary orientation of the dipoles with respect to their plane of motion. Our results show that the tunable dipolar interaction, especially the orientation of the dipoles, can be used to control the direction of stripe phase and its related half-vortex sheets. In addition, it can also be used to obtain a regular arrangement of various topological spin textures, such as meron, circular and cross disgyration spin structures. We point out that such topological defects and regular arrangement of spin structures arise primarily from the long-range and anisotropic nature of

* Correspondence to: National Time Service Center, Chinese Academy of Sciences, Xi'an 710600, China.
E-mail address: xfzhang@ntsc.ac.cn (X.-F. Zhang).

http://dx.doi.org/10.1016/j.aop.2016.10.018

dipolar interaction and its competition with the spin-dependent optical lattices and rotation.

1. Introduction

One of the remarkable aspects of a dilute gas of Bose–Einstein condensate (BEC) is the great success of the mean-field theory governed by the well-known Gross–Pitaevskii (GP) equation. Many of the observed static and dynamics properties of the BEC are usually studied by solving such an equation involving a local term that describes the short-range contact interactions. Recently experimental progress in trapping and cooling of atoms with large magnetic moments, such as ^{52}Cr (^{168}Er or ^{164}Dy) condensate with dominant long-range and anisotropic dipole–dipole interaction (DDI), has launched huge interest in the field of nonlocal nonlinearity, which has been a subject of active investigation in disparate physical systems during the past years [1–5].

Historically, the nonlocal nonlinearity was studied in the physics of plasmas [6] and nematic liquid crystals [7], and also in nonlinear media [8]. Notably, previous studies on dipolar quantum gases have shown that the nonlocal nonlinearity, introduced by DDI, plays a crucial role in the nonlinear dynamics of the system, especially in the physics of soliton and vortex [9,10], and its related topological structures [11–13]. Besides the high degree of control over most of the system parameters, the long-range and anisotropic nature of dipolar quantum gases not only offer researchers to explore regions of parameter space that are difficult to access in a naturally occurring system, but also make the system an ideal candidate for exploring a variety of nonlinear phenomena and the formation of various topological defects and spin structures [14,15].

Recently, it has become possible to produce a two-component BEC, in which the atoms in one component have a magnetic dipole moment and the atoms in the other component are nonmagnetic [16–18]. The major merits of such a system lie in the fact that it not only allows the pattern and topological defects formation without suffering a dipolar collapse, but also offers us an alternative way for exploring the effects of DDI on the non-dipolar condensate. However, previous studies on such a system mainly involved dipoles either perpendicular or parallel to the condensate plane. In addition, in real experiments, designing various types of the optical lattice (OL), such as double-periodic optical superlattice and spin-dependent (rotating or not) OLs, is within current experimental capability [19,20]. More specifically, Han et al. have investigated the half-vortex sheets and domain-wall trains of a two-component BEC without DDI in spin-dependent OLs [21].

Proceeding along these lines, it is then natural to consider a two-component condensate, which consists of both dipolar and scalar atoms confined in spin-dependent OLs, for an arbitrary orientation of the dipoles with respect to the plane of motion of the atoms, which is what we attempt to do in this work. It is shown that the present system, contrary to the non-dipolar case, not only has eyebrowlike spin texture and half-vortex sheet, but also exhibits exotic ground-state structures and regular arrangements of various spin structures, such as self-squeezing, meron, circular and cross disgyration. Furthermore, our results show that the orientation of dipoles constitutes an additional tuning parameter, providing us a unique mechanism for the formation of various topological defects and resulting in rich ground state phases.

2. Formalism

The system considered here is schematically illustrated in Fig. 1. A quasi-two-dimensional (quasi-2D) two-component BEC, each with mass m_i and atom number N_i, is used, where the atoms in component 1 have a magnetic dipole moment and the atoms in component 2 are nonmagnetic. In addition, a magnetic field is applied to fix the direction of the fully polarized magnetic dipoles, which

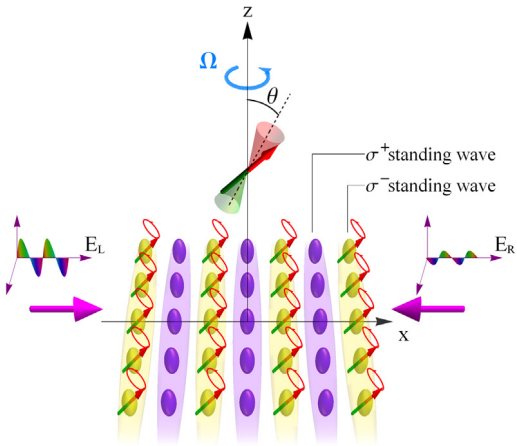

Fig. 1. (Color online) Schematic diagram. The component 1 (yellow) has a dipole moment, which is polarized by an external field and forms an angle θ with the z axis; while component 2 (purple) not. The external potential considered here is a combination of harmonic potential and spin-dependent optical lattices, and each component is confined at the minima of respective optical lattice.

is in the x–z plane and forms an angle θ with the z-axis [22]. Such a system is confined in one-dimensional spin-dependent OLs and subject to a rotation along the z-axis. At mean-field level, the system can be described by the nonlocal GP equation [23]

$$i\hbar\frac{\partial\psi_i(\mathbf{r},t)}{\partial t} = \Big(h_i(\mathbf{r}) + g_{ii}|\psi_i|^2 + g_{i(3-i)}|\psi_{(3-i)}|^2 + \frac{\mu_0\mu_i\mu_{(3-i)}}{4\pi}\int U_{dd}(\mathbf{r})|\psi_{(3-i)}(\mathbf{r}',t)|^2 d\mathbf{r}' + \frac{\mu_0\mu_i^2}{4\pi}\int U_{dd}(\mathbf{r})|\psi_i(\mathbf{r}',t)|^2 d\mathbf{r}'\Big)\psi_i(\mathbf{r},t), \tag{1}$$

where $h_i(\mathbf{r}) = -\frac{\hbar^2}{2m_i}\nabla^2 + V^i_{ext}(\mathbf{r}) - \Omega L_z$, ψ_i is the condensate wave function with normalization $\int d\mathbf{r}|\psi_i(\mathbf{r},t)|^2 = N_i$, $L_z = -i\hbar(x\partial_y - y\partial_x)$ is the z-component of the angular momentum, μ_0 and μ_i are the magnetic permeability of vacuum and the magnetic dipole moment for component i, respectively. For the isotropic contact interactions, $g_{ii} = 2\sqrt{2\pi}\,\hbar^2\, a_{ii}/m_i l_z$ and $g_{i(3-i)} = \sqrt{2\pi}\,\hbar^2\, a_{i(3-i)}/m_R l_z$ with $l_z = \sqrt{\hbar/m\omega_z}$ and $m_R = m_1 m_2/(m_1+m_2)$ being the oscillator length in the z direction and the reduced mass, a_{ii} and $a_{i(3-i)}$ are the corresponding intra- and inter-component scattering lengths, respectively. The long-range and nonlocal DDI potential has the form with

$$U_{dd}(\mathbf{r}-\mathbf{r}') = \frac{1-3\cos^2\Theta}{|\mathbf{r}-\mathbf{r}'|^3}, \tag{2}$$

where Θ is the angle between the polarization direction and the interatom vector $\mathbf{r}-\mathbf{r}'$. The external trapping potential, $V_{ext}(\mathbf{r})$, is assumed to be a combination of harmonic and spin-dependent OLs of the form

$$V^i_{ext}(\mathbf{r}) = \frac{m_i}{2}\omega_\perp^2(x^2+y^2) + V_{oli}, \tag{3}$$

with $\omega_\perp = \omega_x = \omega_y$, $V_{ol1} = I_0\sin^2(kx)$ and $V_{ol2} = I_0\cos^2(kx)$ for components 1 and 2, respectively [20,24]. Here k is the wave vector of the laser light used for the OL potential and I_0 is the potential depth of the lattices. For simplicity, we assume that the two components have the same mass m and the same number of atoms N, and consider only repulsive short-range contact interactions. In addition, we assume component 2 is nondipolar, resulting in zero inter-component dipolar interaction. For dipolar component 1, to compare the dipolar and contact interactions, we define the relative strength

of such two interactions as $\xi_{dd} = \mu_0\mu_1^2 m/(12\pi a_s \hbar^2)$, with dipolar length $a_{dd} = \mu_0\mu_1^2 m/(12\pi \hbar^2)$ and a_s being the three-dimensional s-wave scattering length. In real experiments, this value can be tuned by Feshbach resonance (tuning the s-wave scattering length) and an external field rotation, leading to a large parameter space.

The stationary states of the system can be obtained by using the imaginary-time propagation in Cartesian coordinates [25,26]. The DDI is treated by Fourier transformation in momentum space using a convolution theorem in the usual fashion, which can be written as

$$\Phi(\mathbf{r}, t) = \frac{\mu_0\mu_1^2}{3\sqrt{2\pi}l_z}\mathcal{F}_{2D}^{-1}[\tilde{n}(\mathbf{k}, t)F(\mathbf{k}l_z/\sqrt{2})], \tag{4}$$

here $\mathcal{F}_{2D}$ is the 2D Fourier transform operator and $\tilde{n}(\mathbf{k}, t) = \mathcal{F}_{2D}[n(\mathbf{r}, t)]$. The function $F(\mathbf{q})$ with $\mathbf{q} \equiv \mathbf{k}l_z/\sqrt{2}$ is the k space DDI for the quasi-2D geometry, which consists of two parts coming from polarization perpendicular or parallel to the direction of the dipole tilt. That is $F(\mathbf{q}) = \cos^2(\alpha)F_\perp(\mathbf{q}) + \sin^2(\alpha)F_\parallel(\mathbf{q})$ with α being the angle between $\hat{z}$ and the polarization vector $\hat{d}$. Here $F_\perp(\mathbf{q}) = 2 - 3\sqrt{\pi}qe^{q^2}\mathrm{erfc}(q)$, $F_\parallel(\mathbf{q}) = -1 + 3\sqrt{\pi}(q_d^2/q)e^{q^2}\mathrm{erfc}(q)$, $\mathbf{q}_d$ is the wave vector along the direction of the projection of $\hat{d}$ onto the x–y plane, and erfc is the complementary error function [27,28]. Without loss of generality, we further assume that all the contact interactions are fixed as $g_{11} = g_{22} = g_{12} = g = 1000$, the period and potential depth of the OL are fixed as $\mathrm{T} = \pi$ and $I_0 = 5$. Finally, we work in dimensionless units by introducing the scales characterizing the trapping potential: the length is expressed in units of oscillator length $l_0 = \sqrt{\hbar/m\omega_\perp}$, the time is expressed in units of $t_0 = 1/\omega$, the energy is expressed in units of oscillator energy $\hbar\omega$, and the probability density $|\psi_i|^2$ is expressed in units of $N_i l_0^{-3}$. We start from some proper initial wave-function and propagate it until the fluctuation in the norm of the wave function becomes smaller than 10^{-6}.

3. Topological defects and spin structures

Let us consider the stationary states of the system. As discussed in [21], for the non-dipolar case, straight half-vortex sheets and domain-wall trains emerge as the ground state phases of the system. In what follows we systematically perform numerical simulations for various values of the system parameters to study the ground-state and rotational properties of the system. It is found that the presence of tunable dipolar interactions in component 1 provides a unique mechanism for the formations of various regular arrangements of topological defects and spin structures.

In Fig. 2, we show the typical density distributions of the system for fixed $g = 1000$, $\xi_{dd} = 0.8$, $\Omega = 0.6$, but for different orientations of the dipoles $\theta = 0°, 15°, 30°, 45°, 60°, 90°$. The first three columns correspond to the densities of components 1 and 2, and the total density of these two components, respectively. As shown in Fig. 2, it is clear that not only the density of each component but also the total density of these two components depends sensitively on the orientation of the dipoles. This is obviously different from the non-dipolar case with the same OLs, where the system undergoes phase separation in the form of stripes arranged alternately along the direction of the OLs (*i.e.*, x-axis direction), and the total density of the system is almost unchanged for a large range of parameter sets [21].

When the dipoles are polarized along the z-axis, *i.e.*, $\theta = 0°$, the DDI is purely repulsive and isotropic. As shown in Fig. 2(a), the ground-state density of the system is the well-known stripe phase, where each component is arranged alternately along the direction of the OLs (*i.e.*, x-axis direction). In this case, the net effect of DDI is to increase the number of vortices in component 1 [as shown in Fig. 3(a) for the phase distribution of the system, where its positions are determined by the singularities of the phase], and to enlarge the dipolar cloud. Recall that a two-component system allows the existence of half-quantized vortices, whose winding number is one half of a singly quantized vortex in single-component BEC. We thus refer to these vortices and its related vortex structures as half-quantized vortices and straight half-vortex sheets, respectively [29].

Upon increasing θ to 15°, we find a similar vortex structure since the attractive part of the dipolar interaction is less important. However, it, to some extent, leads to the change of density distribution,

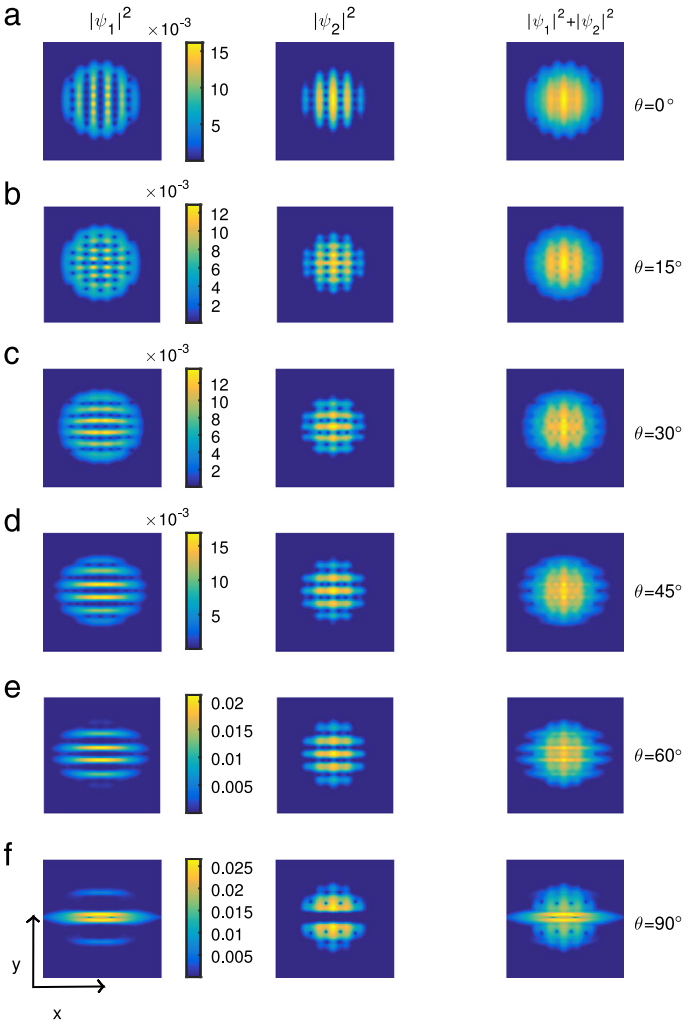

Fig. 2. (Color online) Effects of long-range and anisotropic DDI on the density distributions of the system. The contact interactions are fixed as g = 1000, the strength of DDI $\xi_{dd} = 0.8$, the rotation frequency $\Omega = 0.6$, the period of the optical lattice potential $T = \pi$, and the orientation of the dipoles $\theta = 0^\circ, 15^\circ, 30^\circ, 45^\circ, 60^\circ, 90^\circ$. The size of the frame is 25.6×25.6 in dimensionless unit of $l_0 = \sqrt{\hbar/m\omega_\perp}$.

as shown in Fig. 3(b) for the density difference of these two components. In this case, some high energy atoms can overcome the OL and have a certain tunneling probability, as shown in Figs. 2(b) and 3(b). As θ exceeds 30°, the situation is changed. In this case, the attractive part of the dipole interaction becomes dominant, leading to a change of the direction of the stripe phase, that is, the stripes of each component are arranged alternately perpendicular to the direction of the OLs (*i.e.*, *y*-axis direction). As expected, this phenomenon occurs more obviously for even larger θ, such as $\theta = 45^\circ, 60^\circ$. Typical density and phase distributions of such cases are shown in Figs. 2(c)–(e) and Figs. 3(c)–(e), respectively.

An interesting observation occurs at $\theta = 90^\circ$. In this case, the orientation of the dipoles is parallel to their plane of motion, and the DDI is attractive in the *x*-axis but repulsive in the *y*-axis. The presence of repulsive inter-component interaction, together with this anisotropic and long-range DDI, leads to the self-squeezing of the dipolar component, as shown in Figs. 2(f) and 3(f). This behavior is in a sense

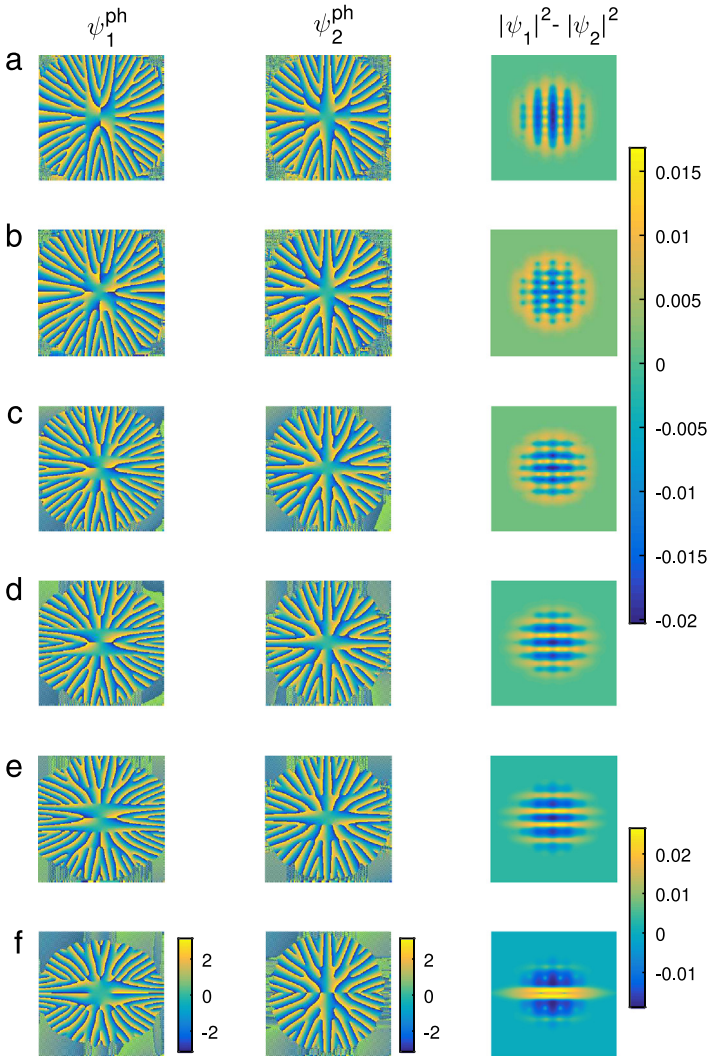

Fig. 3. (Color online) The phase distributions and density difference of the two components for the states represented in Fig. 2. For the phase distributions, value of the phase varies continuously from 0 (blue) to 2π (yellow). The parameters are the same as those in Fig. 2, and the size of the frame is 25.6×25.6 in dimensionless unit of $l_0 = \sqrt{\hbar/m\omega_\perp}$.

reminiscent of the cases in [22], where a single (two)-component dipolar component was considered in anisotropic (isotropic) harmonic potential, respectively.

In principle, rapid rotation will generate more vortices between the stripes of each component. However, it does not change the essential density distribution of the present system, and this holds even for the non-rotational case ($\Omega = 0$), where there is no vortex appearing at all. In addition, the system always shows a similar change of the density profiles over a large range of ξ_{dd}. Hence, the physical mechanism for the change of the direction of the stripes and the self-squeezing, lies in the *anisotropic* nature of DDI and its competition with OLs. Consequently, we can safely conclude that the orientation of the dipoles, which constitutes an additional tuning parameter, can be used to change the direction of the straight half-vortex sheets, and to induce the self-squeezing of the dipolar component, even in the presence of the spin-dependent OLs.

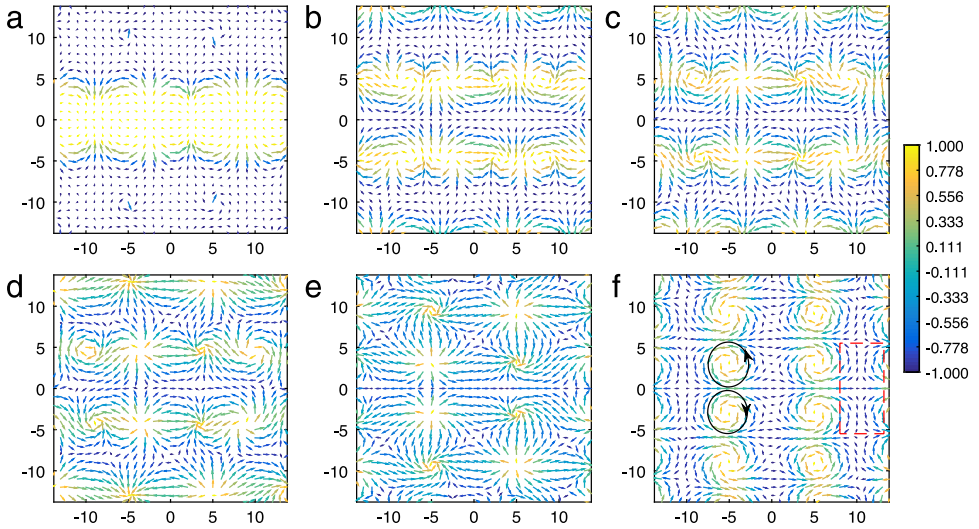

Fig. 4. (Color online) The two-dimensional representations of the pseudospin S projected onto the x–y plane corresponding to the states represented in Fig. 2: (a) $\theta = 90°$; (b) $\theta = 60°$; (c) $\theta = 45°$; (d) $\theta = 30°$; (e) $\theta = 15°$; (f) $\theta = 0°$. The arrows represent the transverse spin vector (S_x, S_y) with length and color representing its magnitude and the values of S_z, which ranges from -1 (blue) to 1 (yellow). In (f), the circular disgyration spin structures are denoted by the black circles with arrows indicating the directions of circulations, and the cross disgyration one is denoted by red dashed rectangle. The other parameters are the same as those in Fig. 2, and the size of the frame is 25.6×25.6 in dimensionless unit of $l_0 = \sqrt{\hbar/m\omega_\perp}$.

Topological spin textures, such as skyrmions (Anderson–Toulouse vortices) and merons (half-skyrmion, Mermin–Ho vortices) play a central role in describing the physics of elementary particles, liquid ^{3}He-A, and BEC [30–35]. For a condensate with an internal spin degree of freedom, the realization and stability of such spin textures have been studied [36,37]. For the dipolar quantum gases, previous studies have shown that dipolar effects in atomic BEC can be used to develop various spin textures [38,39]. Thus, it is also of interest to investigate the pseudospin $\mathbf{S}$ of the system, which manifests itself as the presence of various topological spin structures.

By introducing a normalized complex-valued spinor ϕ, the two-component wave functions can be written as $\psi_{\uparrow\downarrow} = \sqrt{\rho_T(\mathbf{r})}\phi_{\uparrow\downarrow}(\mathbf{r})$ with $\rho_T(\mathbf{r})$ being the total density and the spinor satisfies $|\phi_\uparrow|^2 + |\phi_\downarrow|^2 = 1$. Consequently, the pseudospin vector can be defined as $\mathbf{S} = \phi(\mathbf{r})^T\sigma\phi(\mathbf{r})$ with σ being the Pauli matrix. The explicit expressions of $\mathbf{S} = (S_x, S_y, S_z)$ are given by [40]

$$\begin{aligned} S_x &= (\phi_1^*\phi_2 + \phi_2^*\phi_1) = 2|\phi_1 \parallel \phi_2| \cos(\theta_1 - \theta_2), \\ S_y &= -i(\phi_1^*\phi_2 - \phi_2^*\phi_1) = -2|\phi_1 \parallel \phi_2| \sin(\theta_1 - \theta_2), \\ S_z &= |\phi_1|^2 - |\phi_2|^2, \end{aligned} \tag{5}$$

where $\theta_{1,2}$ is the phase of the wave function $\phi_{\uparrow\downarrow}$ and the modulus of the total spin is $|\mathbf{S}| = 1$.

Fig. 4 shows the two-dimensional representations of pseudospin S projected onto the x–y plane, corresponding to the states represented in Fig. 2 for different orientations of the dipoles. It is easy to see that such spin texture depends very sensitively on the orientation of the dipoles. For $\theta = 90°$ and 60°, we again observe the so-called eyebrowlike spin textures on the domain walls, which was previously observed for the non-dipolar condensate. However, in the present case, due to the long-range and anisotropic nature of DDI, the directions of both the domain wall and eyebrowlike spin texture are changed from the x-axis (parallel to the direction of OLs) to y-axis direction (perpendicular to OLs), as shown in Fig. 4(a) and (b).

Decreasing the orientation angle θ, the eyebrowlike spin textures gradually evolve into the meron and whirling patterns randomly arranged, as shown in Fig. 4(c) for 45°. In addition, by further decreasing θ, such as $\theta = 30°, 15°$, some meron evolves into circular disgyration with

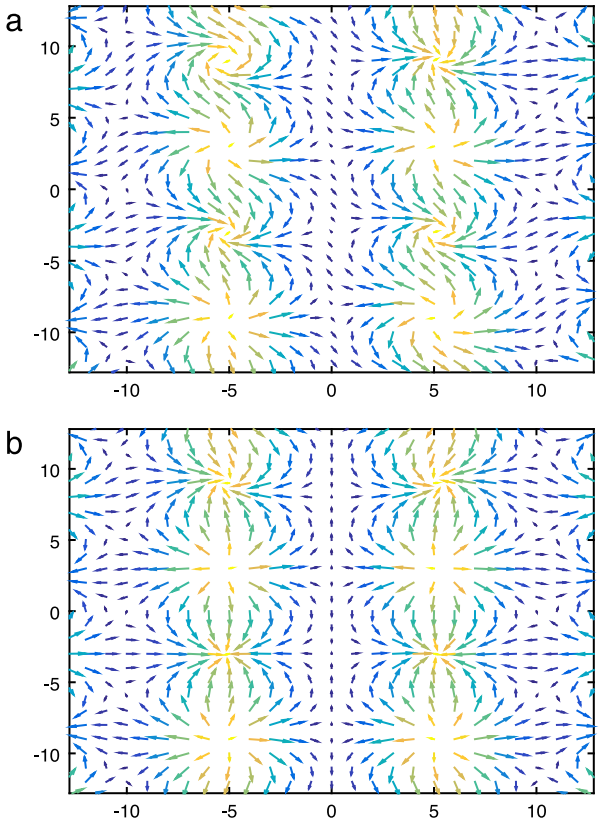

Fig. 5. (Color online) The two-dimensional representations of the pseudospin S projected onto the x–y plane corresponding to the same parameters represented in Fig. 2(f). The profiles (a) and (b) are obtained by the numerical simulation starting from trial wave functions with different global phase difference.

different circulations, as shown in Fig. 4(d) and (e). Eventually, when the orientation of the dipoles is perpendicular to their plane of motion, *i.e.*, $\theta = 0^{\circ}$, *regular* arrangements of circular and cross disgyration spin structures are formed. Typical spin texture of such case is shown in Fig. 4(f), where the circular disgyration spin structures are denoted by the marked black circles with arrows indicating the directions of circulations, and the cross disgyration spin structure is denoted by red dashed rectangle. Furthermore, we note that the Hamiltonian of the system and GP equation (1) are invariant under the gauge transformation $\psi_i \rightarrow \psi_i \exp(i\varphi_i)$ with φ_i being an arbitrary real number. For the same parameters, we obtain other *regular* arrangements of spin structures, as shown in Fig. 5, where their energies are the same as that of Fig. 4(f). Therefore, continuous degenerate states will appear in the present system.

Actually, similar spin structures were previously observed in a spin-1 condensate [31,32,36] and recently in spin–orbit-coupled condensate in the Mott-insulator regime [41], where different types of interactions result in such structures. For the present system, it is necessary to point out the following: (i) in the absence of rotation and only DDI and contact interactions are taken into account, no topological spin structure can be formed; (ii) in the absence of DDI and for the immiscible case with $g_{11}g_{22} < g_{12}^2$, only eyebrowlike spin textures can be formed on the domain walls; (iii) in the absence of DDI and for the miscible case with $g_{11}g_{22} > g_{12}^2$, only *randomly* arranged spin structures can be formed by either increasing the intra-component interaction or lowering the heights of the optical lattices. Consequently, the formations of *regularly* arrangement of spin structures, are essentially due to the intrinsic *long-range* characteristic of DDI and its competition with the spin-dependent OLs and

rotation. From the energetical point of view, the repulsive interaction increases with a decrease of the orientation angle, and it is purely repulsive for $\theta = 0^\circ$. Consequently, regular arrangements of the spin structures, such as meron, circular disgyration, and cross disgyration, are more energetically favorable.

The results presented above can be realized using current experimental setups. The special *two-component* system can be realized by selecting two states in the ground hyperfine manifolds of atomic Cr, Er, or Dy, where components 1 and 2 consist of states with spin projections $m_J = -J$ and $m_J = 0$. The spin-dependent OL potentials can be realized by using two counter propagating blue-detuned laser beams with the same frequency but perpendicular linear polarization vectors [24]. For the tunable DDI, the orientation of dipoles can be manipulated by an external polarized field, and its magnitude can be controlled by means of rotating another orienting field [42]. Hence, the parameters used in this study are feasible in current experiments. Finally, the topological spin textures are experimentally observable by magnetization-sensitive phase-contrast imaging technique.

4. Conclusion

In conclusion, we have studied the ground-state phases of a rotating binary dipolar condensate, which consists of both dipolar and non-dipolar components and is confined in spin-dependent OLs, for an arbitrary orientation of the polarization axis with respect to their plane of motion. We show that the tunable dipolar interaction, especially the orientation of the dipoles, can be used to control the direction of the stripe phase and its related half-vortex sheets. In addition, when the orientation of the dipoles is aligned along the x-axis, we also find the well-known self-induced squeezing of the dipolar component along the y-axis direction, even in the presence of spin-dependent optical lattices in the x-axis direction. Furthermore, we observe a variety of nontrivial topological defects such as eyebrowlike spin texture, meron, circular disgyration, and cross disgyration, and find that regular arrangements of such spin textures can be obtained by changing the orientation of the dipoles.

The underlying physics of the formation of such topological defects and spin structures is the competition among DDI, rotation, and the spin-dependent OLs. Our results open up alternative ways for the formation of various topological defects and spin structures in future experiments.

Acknowledgments

This work is supported by NSF of China under Grants Nos. 61025023, 11547126; the NMFSEID under Grant No. 61127901. X.F. Zhang is also supported by the fund of the CAS for the "Western Light" Talent Cultivation Plan under Grant No. 2012ZD02, and Youth Innovation Promotion Association of CAS under Grant No. 2015334. H. Saito is supported by JSPS KAKENHI under Grant Nos. JP16K05505, JP26400414, and JP25103007.

References

[1] T. Lahaye, T. Koch, B. Frohlich, M. Fattori, J. Metz, A. Griesmaier, S. Giovanazzi, T. Pfau, Nature 448 (2007) 672–675.
[2] T. Koch, T. Lahaye, J. Metz, B. Frohlich, A. Griesmaier, T. Pfau, Nat. Phys. 4 (2008) 218–222.
[3] M. Lu, S.H. Youn, B.L. Lev, Phys. Rev. Lett. 104 (2010) 063001.
[4] M. Lu, N.Q. Burdick, S.H. Youn, B.L. Lev, Phys. Rev. Lett. 107 (2011) 190401.
[5] K. Aikawa, A. Frisch, M. Mark, S. Baier, A. Rietzler, R. Grimm, F. Ferlaino, Phys. Rev. Lett. 108 (2012) 210401.
[6] A.G. Litvak, V.A. Mironov, G.M. Fraiman, A.D. Yunakovskii, Sov. J. Plasma Phys. 1 (1975) 60–71.
[7] M. Peccianti, C. Conti, G. Assanto, A. De Luca, C. Umeton, Nature 432 (2004) 733–737.
[8] A.S. Desyatnikov, A.A. Sukhorukov, Y.S. Kivshar, Phys. Rev. Lett. 95 (2005) 203904.
[9] M. Klawunn, R. Nath, P. Pedri, L. Santos, Phys. Rev. Lett. 100 (2008) 240403.
[10] T. Lahaye, C. Menotti, L. Santos, M. Lewenstein, T. Pfau, Rep. Progr. Phys. 72 (2009) 126401.
[11] J. Zhang, H. Zhai, Phys. Rev. Lett. 95 (2005) 200403.
[12] N.R. Cooper, E.H. Rezayi, S.H. Simon, Phys. Rev. Lett. 95 (2005) 200402.
[13] S. Yi, H. Pu, Phys. Rev. A 73 (2006) 061602.
[14] M.A. Baranov, Phys. Rep. 464 (2008) 71–111.
[15] M. Tsubota, M. Kobayashi, H. Takeuchi, Phys. Rep. 522 (2013) 191–238.
[16] H. Saito, Y. Kawaguchi, M. Ueda, Phys. Rev. Lett. 102 (2009) 230403.
[17] Y. Zhao, J. An, C.D. Gong, Phys. Rev. A 87 (2013) 013605.

[18] W.E. Shirley, B.M. Anderson, C.W. Clark, R.M. Wilson, Phys. Rev. Lett. 113 (2014) 165301.
[19] K. Góral, L. Santos, M. Lewenstein, Phys. Rev. Lett. 88 (2002) 170406.
[20] O. Mandel, M. Greiner, A. Widera, T. Rom, T.W. Hänsch, I. Bloch, Phys. Rev. Lett. 91 (2003) 010407.
[21] W. Han, S. Zhang, J. Jin, W.M. Liu, Phys. Rev. A 85 (2012) 043626.
[22] F. Malet, T. Kristensen, S.M. Reimann, G.M. Kavoulakis, Phys. Rev. A 83 (2011) 033628.
[23] S.K. Adhikari, Phys. Phys. Rev. A 89 (2014) 013630.
[24] O. Mandel, M. Greiner, A. Widera, T. Rom, T.W. Hänsch, I. Bloch, Nature 425 (2003) 937–940.
[25] W. Bao, Y. Cai, H. Wang, J. Comput. Phys. 229 (2010) 7874–7892.
[26] R.K. Kumar, L.E. Young-S, D. Vudragović, A. Balaẑ, P. Muruganandamd, S.K. Adhikari, Comput. Phys. Comm. 195 (2015) 117–128.
[27] R. Nath, P. Pedri, L. Santos, Phys. Rev. Lett. 102 (2009) 050401.
[28] B.C. Mulkerin, R.M.W. van Bijnen, D.H.J. O' Dell, A.M. Martin, N.G. Parker, Phys. Rev. Lett. 111 (2013) 170402.
[29] M. Eto, K. Kasamatsu, M. Nitta, H. Takeuchi, M. Tsubota, Phys. Rev. A 83 (2011) 063603.
[30] N.D. Mermin, T.L. Ho, Phys. Rev. Lett. 36 (1976) 594–597.
[31] T.L. Ho, Phys. Rev. Lett. 81 (1998) 742–745.
[32] T. Ohmi, K. Machida, J. Phys. Soc. Japan 67 (1998) 1822–1825.
[33] S.K. Yip, Phys. Rev. Lett. 83 (1999) 4677–4681.
[34] R. Blaauwgeers, V.B. Eltsov, M. Krusius, J.J. Ruohio, R. Schanen, G.E. Volovik, Nature 404 (2000) 471–473.
[35] U.Al Khawaja, H.T.C. Stoof, Nature 11 (2001) 918–920.
[36] T. Mizushima, K. Machida, T. Kita, Phys. Rev. Lett. 89 (2002) 030401.
[37] C.M. Savage, J. Ruostekoski, Phys. Rev. Lett. 91 (2003) 010403.
[38] L. Santos, T. Pfau, Phys. Rev. Lett. 96 (2006) 190404.
[39] Y. Kawaguchi, H. Saito, M. Ueda, Phys. Rev. Lett. 98 (2007) 110406.
[40] K. Kasamatsu, M. Tsubota, M. Ueda, Phys. Rev. A 71 (2005) 043611.
[41] J. Radić, A. Di Ciolo, K. Sun, V. Galitski, Phys. Rev. Lett. 109 (2012) 085303.
[42] S. Giovanazzi, A. Görlitz, T. Pfau, Phys. Rev. Lett. 89 (2002) 130401.